Hindawi Publishing Corporation
Shock and Vibration
Volume 2015, Article ID 947937, 16 pages
http://dx.doi.org/10.1155/2015/947937

Research Article

Damping Force Tracking Control of MR Damper System Using a New Direct Adaptive Fuzzy Controller

Xuan Phu Do, Kruti Shah, and Seung-Bok Choi

Smart Structures and Systems Laboratory, Department of Mechanical Engineering, Inha University, Incheon 402-751, Republic of Korea

Correspondence should be addressed to Seung-Bok Choi; seungbok@inha.ac.kr

Received 24 October 2014; Revised 4 January 2015; Accepted 5 January 2015

Academic Editor: Sakdirat Kaewunruen

This paper presents a new direct adaptive fuzzy controller and its effectiveness is verified by investigating the damping force tracking control of magnetorheological (MR) fluid based damper (MR damper in short) system. In the formulation of the proposed controller, a model of interval type 2 fuzzy controller is combined with the direct adaptive control to achieve high performance in vibration control. In addition, H^{∞} (H infinity) tracking technique is used in building a model of the direct adaptive fuzzy controller in which an enhanced iterative algorithm is combined with the fuzzy model. After establishing a closed-loop control structure to achieve high control performance, a cylindrical MR damper is adopted and damping force tracking results are obtained and discussed. In addition, in order to demonstrate the effectiveness of the proposed control strategy, two existing controllers are modified and tested for comparative work. It has been demonstrated from simulation and experiment that the proposed control scheme provides much better control performance in terms of damping force tracking error. This leads to excellent vibration control performance of the semiactive MR damper system associated with the proposed controller.

1. Introduction

Recently, magnetorheological (MR) fluids based devices are actively studied and some of devices such as shock absorber for passenger vehicles are commercialized. Many MR devices or MR systems especially are popularized in the field of aerospace, ship, automobile, and civil engineering for effective control of unwanted vibrations. It is well known that MR fluid is considered as one of smart fluids in which the rheological properties can be controlled by external stimuli such as magnetic field. On the other hand, the development of new control system for MR devices or systems is also continuously undertaking in which the objective goal is to guarantee both stability and robustness against disturbances or/and uncertainties. Based on this objective, several types of robust controllers have been developed in both indirect adaptive control and direct adaptive control manners. A model of direct adaptive control for output tracking was studied in [1] where H infinity tracking technique was used for adaptive model. An adaptive fuzzy control for MIMO system was presented in [2] in which the Lyapunov function and mean-value theorem were combined with a fuzzy model to build adaptive model. An observer of adaptive fuzzy controller was presented in [3] in which the back-stepping design and the supply changing function technique were applied. An input saturation problem was treated with adaptive feedback fuzzy control in [4] where the back-stepping technique and Lyapunov function were used in building the adaptive model. A direct adaptive control using type 2 fuzzy model was presented in [5] where H infinity tracking technique was applied to attenuate the fuzzy approximation error and the system uncertainty. The linear matrix inequality fuzzy Lyapunov method was also studied in [6] which concentrated on modeling errors between real system and fuzzy model. Recently, a novel of adaptive sliding mode control was developed by authors in [7] in which a sliding mode controller and Lyapunov method were used for high control performance. Vibration control of MR damper using an adaptive neurofuzzy inference system was also conducted by authors in [8].

In application of feedback/feed-forward controls for tracking force of MR devices, there are several researches.

An idealized hysteretic model for MR was studied in [9] using a nonlinear hysteretic bi-viscous model. For seismic response reduction, a clipped-optimal control using acceleration feedback was studied in [10] in which the properties of MR damper were tested to provide good vibration control performance. A model of MR damper for bridge application was derived in [11] using a semiactive tuned mass damper. A combination of the feed-forward and feedback control was also presented in [12] for torque control of MR brake. On the other hand, in research of interval type 2 fuzzy model (IT2FM), many studies on the development of controller type have been undertaken. A comprehensive research about type-reduction of three groups, Karnik-Mendel (KM), closed-form representation, and combined KM-closed form representation, were presented in [13]. In this study, EIASC (Enhanced Iterative Algorithm with Stopping Condition), Wu-Tan (WT) algorithm, and Nie-Tan (NT) algorithm were used to reduce calculation cost. Another research concentrating on KM algorithm in IT2FM was studied in [14] in which all methods were evaluated based on KM method. In order to solve the bottle-neck problem in calculating of type reduction of IT2FM, a new method of combination of KM and NT method was presented in [15]. It is recognized from the above survey that the development of a new adaptive fuzzy controller which is robust to disturbances or/and uncertainties is a hot issue in many control systems including MR device or MR systems. The development of new IT2FM especially is a new horizon in design of new controllers to guarantee both stability and robustness against disturbances and uncertainties [13–15].

Consequently, the technical originality of this work is to propose a new direct adaptive fuzzy controller using both IT2FM and adaptation method based on H-infinity tracking technique for the robust damping force tracking control of a cylindrical MR damper. Thus, a final goal is to demonstrate superior control performances of the proposed new direct adaptive fuzzy controller compared with two existing adaptive fuzzy controllers [1, 2]. In order to clarify the difference from the previous work done by the authors [7], it is noted here that the previous study deals with the indirect adaptive fuzzy controller, while current study treats the direct adaptive fuzzy controller whose structure is much different from the indirect method. In order to achieve the final goal of this work, as a first step, a new interval type 2 fuzzy control system is formulated. Then, a new type of adaptive controller is designed based on H infinity tracking technique and Lyapunov method. Based on the mathematical model, a closed-loop control structure is built and experimentally realized for a small-sized MR damper. MR fluid used in this work is manufactured in the laboratory using plate-like iron particles. Its field-dependent rheological characteristics are different from general MR fluid containing spherical iron particles. In order to demonstrate superior control performance of the proposed controller, both tracking control of desired damping force of MR damper and vibration control performance are evaluated and compared with existing two controllers.

2. Interval Type 2 Fuzzy Logic System and NT Algorithm

The model of interval type 2 fuzzy logic system (IT2FLS) has been developed from the type 1 fuzzy logic system (T1FLS). The structure of IT2FLS includes five components: fuzzifier, rule base, inference engine, type reducer, and defuzzifier. The rule base of IT2FLS can be expressed as follows:

$$RB^j\text{: If } a_1 \text{ is } \mathbf{A_1^j} \text{ and} \ldots \text{and } a_n \text{ is } \mathbf{A_n^j} \text{ Then } B^j, \tag{1}$$

where $\mathbf{A_i^j}$ $(i = 1, \ldots, n;\ j = 1, \ldots, m)$ are fuzzy sets and $\mathbf{B^j} = b^j$ is the centroid of a consequent IT2FLS.

In this study, NT algorithm is utilized for finding output of IT2FM. In general, NT algorithm shows the best algorithm in calculation with minimum computational cost. Hence, the application of NT algorithm will save time of fuzzy calculation. The relationship between NT algorithm and IT2FM is shown in Figure 1. The defuzzification of the IT2FLS-NT is calculated from several steps as follows.

Step 1. Set up input vector $a_v = (a_1, a_2, \ldots, a_n)$. This vector is also vector state of the system whose component a_i is defined as $a_i = \mathbf{A_i^j}$.

Step 2. Find $\mathbf{A_i^j} = [\underline{\mu}(a_i), \overline{\mu}(a_i)]$, where $\underline{\mu}(a_i)$ is lower value and $\overline{\mu}(a_i)$ is upper value of IT2FLS a_i.

Step 3. Calculate lower and upper firing values of IT2FLS $[\underline{f}_j, \overline{f}_j] = [\prod_{i=1}^n \underline{\mu}(a_i), \prod_{i=1}^n \overline{\mu}(a_i)]$ where $\underline{f}_j$ is lower firing value and $\overline{f}_j$ is upper firing value.

Step 4. Use NT algorithm for calculating of $[y_l; y_u]$. Here y_l is lower interval type 1 value and y_u is upper interval type 1 value given by

$$y_l = \frac{\sum_{j=1}^m \underline{f}^j b^j}{\sum_{j=1}^m \left(\underline{f}^j + \overline{f}^j\right)}; \qquad y_u = \frac{\sum_{j=1}^m \overline{f}^j b^j}{\sum_{j=1}^m \left(\underline{f}^j + \overline{f}^j\right)}. \tag{2}$$

Step 5. Calculate defuzzification y_0 of IT2FLS as follows:

$$y_0 = y_l + y_u = \boldsymbol{\theta}^T \boldsymbol{\xi}_\mathbf{l} + \boldsymbol{\theta}^T \boldsymbol{\xi}_\mathbf{u}, \tag{3}$$

where $\boldsymbol{\theta} = \lfloor b^1, b^2, \ldots, b^m \rfloor$, $\boldsymbol{\xi}_\mathbf{l} = \lfloor \xi_l^1, \xi_l^2, \ldots, \xi_l^m \rfloor$, and $\boldsymbol{\xi}_\mathbf{u} = \lfloor \xi_u^1, \xi_u^2, \ldots, \xi_u^m \rfloor$. It is remarked that $\boldsymbol{\theta}$ is consequent vector and $\boldsymbol{\xi}_\mathbf{l}$, $\boldsymbol{\xi}_\mathbf{u}$ are lower and upper consequent membership vectors, respectively.

3. New Direct Adaptive Fuzzy Controller

Consider a nonlinear system is governed by the following equation:

$$\dot{\mathbf{x}} = \mathbf{f}(\mathbf{x}) + \mathbf{g}(\mathbf{x})\, u(t) + \mathbf{d}(\mathbf{t}), \tag{4}$$

where $\mathbf{f}(\mathbf{x}) \in R^n$ and $\mathbf{g}(\mathbf{x}) \in R^n$ are two unknown nonlinear function vectors, $u(t) \in R^1$ is control function, $\mathbf{d}(\mathbf{t}) \in R^n$ is an external disturbance vector, $|\mathbf{d}(\mathbf{t})| \leq \boldsymbol{\delta}\mathbf{d}$, where $\boldsymbol{\delta}\mathbf{d} \in R^n$ is upper bound of $\mathbf{d}(\mathbf{t})$, and $\mathbf{x} = [x_1, x_2, \ldots, x_n] = [x_1, \dot{x}_1, \ldots, x_1^{(n-1)}]^T \in R^n$ is the state vector of the system. The function $\mathbf{f}(\mathbf{x})$ and $\mathbf{g}(\mathbf{x})$ can be expressed in two parts. One is a nominal function and the other is unknown bounded uncertainty as follows:

$$\begin{aligned} \mathbf{f}(\mathbf{x}) &= \mathbf{f_0}(\mathbf{x}) + \boldsymbol{\delta}\mathbf{f}(\mathbf{x}); \quad 0 < |\boldsymbol{\delta}\mathbf{f}(\mathbf{x})| < \|\boldsymbol{\delta}\mathbf{f}\|_\infty, \\ \mathbf{g}(\mathbf{x}) &= \mathbf{g_0}(\mathbf{x}) + \boldsymbol{\delta}\mathbf{g}(\mathbf{x}); \quad 0 < |\boldsymbol{\delta}\mathbf{g}(\mathbf{x})| < \|\boldsymbol{\delta}\mathbf{g}\|_\infty, \end{aligned} \tag{5}$$

where $\mathbf{f_0}(\mathbf{x}) = [x_2, \ldots, x_n, f_0]^T$, $\mathbf{g_0}(\mathbf{x}) = [0, \ldots, 0, g_0]^T$, $\boldsymbol{\delta}\mathbf{f} = [0, 0, \ldots, \delta f_0]^T$, and $\boldsymbol{\delta}\mathbf{g} = [0, 0, \ldots, \delta g_0]^T$. $\boldsymbol{\delta}\mathbf{f}$ and $\boldsymbol{\delta}\mathbf{g}$ are two positive vectors. Hence, the system (4) can be rewritten as

$$\dot{\mathbf{x}} = \mathbf{f_0}(\mathbf{x}) + \mathbf{g_0}(\mathbf{x})\, u(t) + \mathbf{D}, \tag{6}$$

where $\mathbf{D} = \boldsymbol{\delta}\mathbf{f} + \boldsymbol{\delta}\mathbf{g}u(t) + \mathbf{d}(\mathbf{t})$ is uncertain part (disturbance) which can be redefined as $\mathbf{D} = [0, 0, \ldots, D_0]^T$. Then, the relationship between system (6) and IT2FLS is determined based on (3) as follows:

$$\begin{aligned} \mathbf{f_{00}}(\mathbf{x}) &= \mathbf{f_0}(\mathbf{x})\, y_0 = \boldsymbol{\theta}_\mathbf{f}\boldsymbol{\xi}_\mathbf{f}, \\ \mathbf{g_{00}}(\mathbf{x}) &= \mathbf{g_0}(\mathbf{x})\, y_0 = \boldsymbol{\theta}_\mathbf{g}\boldsymbol{\xi}_\mathbf{g}, \end{aligned} \tag{7}$$

where $\boldsymbol{\theta}_\mathbf{f} = [\boldsymbol{\theta}_\mathbf{f}^\mathbf{l}, \boldsymbol{\theta}_\mathbf{f}^\mathbf{u}]^\mathbf{T}$ and $\boldsymbol{\theta}_\mathbf{g} = [\boldsymbol{\theta}_\mathbf{g}^\mathbf{l}, \boldsymbol{\theta}_\mathbf{g}^\mathbf{u}]^\mathbf{T}$, $\boldsymbol{\xi}_\mathbf{f} = \boldsymbol{\xi}_\mathbf{g} = [\boldsymbol{\xi}_\mathbf{l}, \boldsymbol{\xi}_\mathbf{u}]$. Note that $\boldsymbol{\theta}_\mathbf{f}$, $\boldsymbol{\theta}_\mathbf{g}$ are the centroids of consequent vectors and $\boldsymbol{\xi}_\mathbf{f}$, $\boldsymbol{\xi}_\mathbf{g}$ are consequent membership vectors of $\mathbf{f}$, $\mathbf{g}$, respectively. The difference between a desired output x_d and the measure output x is defined by $e = x_d - x$. Thus, the error vector for the system is defined as $\mathbf{E} = [e_0, e_1, e_2, \ldots, e_{n-1}] = [e, \dot{e}, \ddot{e}, \ldots, e^{(n-1)}]$, and a vector $\mathbf{K} = [k_n, k_{n-11}, k_{n-2}, \ldots, k_0]$ is the chosen coefficients such that all of the roots of the polynomial $\sigma^n + k_{n-1}\sigma^{n-1} + k_{n-2}\sigma^{n-2} + \cdots + k_0$ are located in the open left-half complex plane [1, 2].

In relation with fuzzy control, by assuming the disturbance of a direct adaptive fuzzy control is expressed as follows:

$$u = \frac{1}{g_f}\left(-f_{00}(x) + \dot{x}_d + \mathbf{K}^\mathbf{T}\mathbf{E}\right), \tag{8}$$

where g_f is a fuzzified value of g. Using (6) and (8), the derivative of $\mathbf{E}$ is expressed as follows:

$$\dot{\mathbf{E}} = \dot{\mathbf{x}}_\mathbf{d} - \dot{\mathbf{x}} = \boldsymbol{\Lambda}_\mathbf{1}\mathbf{E} + \boldsymbol{\Lambda}_\mathbf{2}\left[\left(g_f - g\right)u + \left(f_{00}(x) - f(x)\right)\right], \tag{9}$$

where

$$\boldsymbol{\Lambda}_\mathbf{1} = \begin{bmatrix} 0 & 1 & 0 & \cdots & \cdots & 0 \\ 0 & 0 & 1 & \cdots & \cdots & 0 \\ \vdots & \vdots & \vdots & \vdots & \vdots & \vdots \\ 0 & 0 & 0 & \cdots & \cdots & 1 \\ -k_n & -k_{n-1} & -k_{n-2} & \cdots & \cdots & -k_1 \end{bmatrix}, \qquad \boldsymbol{\Lambda}_\mathbf{2} = \begin{bmatrix} 0 \\ 0 \\ \vdots \\ 0 \\ 1 \end{bmatrix}. \tag{10}$$

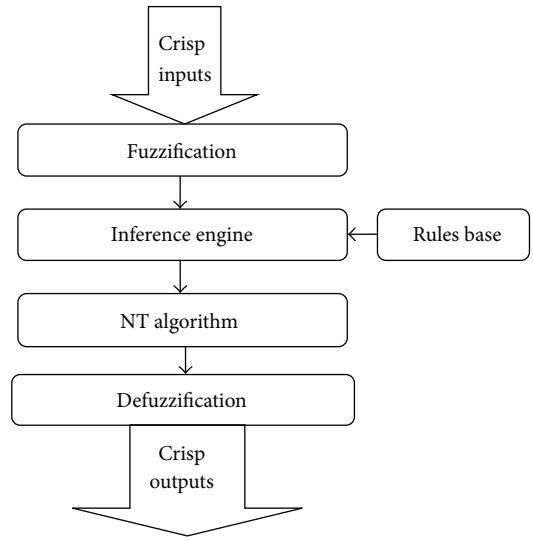

Figure 1: Relationship between IT2FLS model and NT algorithm.

Now, define the minimum approximation error as follows:

$$w = \left(f_{00}^*(x) - f(x)\right) + g_f u. \tag{11}$$

Then, substituting (11) into (9) yields the following equation:

$$\dot{\mathbf{E}} = \boldsymbol{\Lambda}_\mathbf{1}\mathbf{E} + \boldsymbol{\Lambda}_\mathbf{2}\left[\left(\theta_f^* - \theta_f\right)\xi_f - gu + w\right]. \tag{12}$$

Let $\gamma_f = (\theta_f^* - \theta_f)$. From (12), the equivalence control u_1 is defined as

$$u_1 = \frac{1}{g}\left(\widehat{\gamma}_f\xi_f\right), \tag{13}$$

where $\widehat{\gamma}_f$ is the estimates of γ_f. It is noteworthy that the equation u_1 is established without the minimum approximation error w. Due to the presence of fuzzy approximation error and equivalent control term, using only u_1 is not sufficient to ensure the stability of the closed-loop system. Therefore, it is necessary to add a robust compensator to deal with it as follows:

$$u_2 = \Gamma\xi_{fz}\frac{1}{g}\mathbf{E}^\mathbf{T}\mathbf{P}\boldsymbol{\Lambda}_\mathbf{2}, \tag{14}$$

where Γ is an adaptive parameter, and $\mathbf{P} = \mathbf{P}^\mathbf{T} \geq 0$ is a solution of the following Riccati-like equation:

$$\mathbf{P}\boldsymbol{\Lambda}_\mathbf{1} + \boldsymbol{\Lambda}_\mathbf{1}^\mathbf{T}\mathbf{P} + \mathbf{Q} - \Gamma\xi_{fz}\mathbf{P}\boldsymbol{\Lambda}_\mathbf{2}\boldsymbol{\Lambda}_\mathbf{2}^\mathbf{T}\mathbf{P} + \rho\mathbf{P}\boldsymbol{\Lambda}_\mathbf{2}\boldsymbol{\Lambda}_\mathbf{2}^\mathbf{T}\mathbf{P} = 0, \tag{15}$$

where $\rho \geq \Gamma$, ρ is a prescribed attenuation level, and $\mathbf{Q} = \mathbf{Q}^\mathbf{T} \geq 0$, ξ_{fz} is consequent membership value of the IT2FLS. The resulting fuzzy control is determined as follows:

$$u = u_1 + u_2 = \frac{1}{g}\left(\widehat{\gamma}_f\xi_f\right) + \Gamma\xi_{fz}\frac{1}{g}\mathbf{E}^\mathbf{T}\mathbf{P}\boldsymbol{\Lambda}_\mathbf{2}. \tag{16}$$

By substituting (16) into (12), (16) can be rewritten as

$$\dot{\mathbf{E}} = \mathbf{\Lambda_1 E} + \mathbf{\Lambda_2}\left[\tilde{\gamma}_f \xi_f - \Gamma \xi_{fz} \mathbf{E^T P \Lambda_2} + w\right], \tag{17}$$

where $\tilde{\gamma}_f = \gamma_f - \hat{\gamma}_f$.

Now, in order to prove the stability of the control system, consider the Lyapunov function candidate as follows:

$$V = \frac{1}{2}\mathbf{E^T P E} + \frac{1}{2\alpha_1}\tilde{\gamma}_f^2 + \frac{1}{2\alpha_2}\Gamma^2. \tag{18}$$

Then, the derivative of (18) is expressed as follows:

$$\begin{aligned}\dot{V} = &-\frac{1}{2}\mathbf{E^T Q E} - \rho \mathbf{E^T P \Lambda_2 \Lambda_2^T P E} \\ &+ \left(\frac{1}{\alpha_2}\dot{\Gamma}\Gamma - \frac{1}{2}\xi_{fz}\Gamma \mathbf{E^T P \Lambda_2 \Lambda_2^T P E}\right) \\ &+ \frac{1}{2}\left(w^T \mathbf{\Lambda_2^T P E} + \mathbf{E^T P \Lambda_2} w\right) \\ &+ \frac{1}{\alpha_1}\left(\alpha_1 \mathbf{E^T P \Lambda_2} \xi_f + \dot{\tilde{\gamma}}_f\right)\tilde{\gamma}_f.\end{aligned} \tag{19}$$

From (19), adaptation laws are established as follows:

$$\dot{\tilde{\gamma}}_f = -\alpha_1 \mathbf{E^T P \Lambda_2} \xi_f, \qquad \dot{\Gamma} = \frac{\alpha_2}{2}\xi_{fz}\mathbf{E^T P \Lambda_2 \Lambda_2^T P E}. \tag{20}$$

Applying (20), (19) is determined as follows:

$$\dot{V} \le -\frac{1}{2}\mathbf{E^T Q E} + \frac{1}{4\rho}w^2. \tag{21}$$

By integrating (21) from $t = 0$ to $t = T$, the following equation is obtained:

$$V(T) - V(0) + \frac{1}{2}\int_0^T \mathbf{E^T Q E}\, dt - \frac{1}{4\rho}\int_0^T w^2 dt \le 0, \tag{22}$$

where $V(0) = (1/2)\mathbf{E^T}(0)\mathbf{PE}(0) + (1/2\alpha_1)\tilde{\gamma}_f^2(0) + (1/2\alpha_2)\Gamma^2(0)$. The group $[V(T) - V(0)]$ is always more than or equal to zero value. Hence, from (22), the remained group $[(1/2)\int_0^T \mathbf{E^T Q E}\, dt - (1/4\rho)\int_0^T w^2\, dt]$ is analyzed as follows:

$$\frac{1}{2}\int_0^T \mathbf{E^T Q E}\, dt \le \frac{1}{2}\left\|\mathbf{E_Q}\right\|^2 \le \frac{1}{4\rho}\int_0^T w^2 dt \le \left(\frac{1}{2\sqrt{\rho}}\right)^2 \|w\|^2. \tag{23}$$

Since the value is set by $\rho > 0$ and $Q > 0$, the error of matrix $\mathbf{E}$ and the gain of w must be equal to or less than $(1/2\sqrt{\rho})$. Hence, the H infinity tracking form is satisfied [2, 16], and then (21) is always less than zero value (Lyapunov stability). Now, from the boundedness of parameters of $\tilde{\gamma}_f$, Γ is guaranteed by closed sets defined as follows:

$$\begin{gathered}\Omega_1 = \left\{\tilde{\gamma}_f \mid \left\|\tilde{\gamma}_f\right\| \le L_f\right\}, \qquad \Omega_2 = \left\{\Gamma \mid \|\Gamma\| \le L_\Gamma, \Gamma\xi_{fz} \le \rho\right\}, \\ \Omega_{\delta 1} = \left\{\tilde{\gamma}_f \mid \left\|\tilde{\gamma}_f\right\| \le L_f + \delta_1\right\}, \\ \Omega_{\delta 2} = \left\{\Gamma \mid \|\Gamma\| \le L_\Gamma + \delta_2, \Gamma\xi_{fz} + \delta_3 \le \rho + \delta_2\right\},\end{gathered} \tag{24}$$

where L_f, L_Γ, δ_1, δ_2 are the choosing parameters. Hence the adjusted adaptation laws are redefined as

$$\dot{\tilde{\gamma}}_f = \begin{cases} -\alpha_1 \mathbf{E^T P \Lambda_2} \xi_f \\ \quad \text{if } \left\|\tilde{\gamma}_f\right\| < L_f \text{ or } \left(\left\|\tilde{\gamma}_f\right\| = L_f, \mathbf{E^T P \Lambda_2} \xi_f \tilde{\gamma}_f \ge 0\right) \\ -\alpha_1 \mathbf{E^T P \Lambda_2} \xi_f + \alpha_1 \dfrac{\left(\left\|\tilde{\gamma}_f\right\|^2 - L_f\right)\mathbf{E^T P \Lambda_2} \xi_f \tilde{\gamma}_f}{\delta_1 \left\|\tilde{\gamma}_f\right\|^2} \\ \quad \text{if } \left\|\tilde{\gamma}_f\right\| = L_f,\ \mathbf{E^T P \Lambda_2} \xi_f \tilde{\gamma}_f < 0, \end{cases} \tag{25}$$

$$\dot{\Gamma} = \begin{cases} \dfrac{\alpha_2}{2}\mathbf{E^T P \Lambda_2 \Lambda_2^T P E} \xi_{fz} \\ \quad \text{if } \|\Gamma\| < L_\Gamma \\ \quad \text{or } \left(\|\Gamma\| = L_\Gamma + \delta_2, \mathbf{E^T P \Lambda_2 \Lambda_2^T P E} \xi_{fz}\Gamma \ge 0\right) \\ \dfrac{\alpha_2}{2}\mathbf{E^T P \Lambda_2 \Lambda_2^T P E} \xi_{fz} \\ \quad -\alpha_2 \dfrac{\left(\|\Gamma\|^2 - L_\Gamma\right)\mathbf{E^T P \Lambda_2 \Lambda_2^T P E} \xi_{fz}\Gamma}{\delta_2 \|\Gamma\|^2} \\ \quad \text{if } \|\Gamma\| = \rho,\ \mathbf{E^T P \Lambda_2 \Lambda_2^T P E} \xi_{fz}\Gamma < 0. \end{cases} \tag{26}$$

To observe the states of system, an observer for the nonlinear system is needed to converge the estimated state of $\tilde{x}(t)$. In this work, the observer is constructed by the Luenberger observer [17] which is defined as follows:

$$\dot{\tilde{\mathbf{x}}}(\mathbf{t}) = \mathbf{f}(\tilde{\mathbf{x}}(\mathbf{t})) + \mathbf{g}\hat{u}(t) + \left[\mathbf{Q_{ob}}(\tilde{\mathbf{x}}(\mathbf{t}))\right]^{-1}\mathbf{W}\left[y(t) - \tilde{y}(t)\right], \tag{27}$$

where $\mathbf{W} = [W_1, W_2, \ldots, W_n]$ is a finite gain vector, $\mathbf{W} \in R^n$, $\mathbf{Q_{ob}}$ is the observability matrix of the system. From the above analysis, the closed-loop of the proposed controller is shown in Figure 2. In Figure 2, adaptation laws use output of IT2FLS-NT model and error of system for calculating adaptive values of f and Γ. These values are input of fuzzy controller u which is input of observer and plant modules. Output of plant is input of IT2FLS-NT model and base for finding error of system which is also input of IT2FLS-NT model. Value of output observer is also base for calculating error of system.

4. MR Fluid and MR Damper

4.1. New MR Fluid. As mentioned in Introduction, MR fluid is suspension of microsized magnetic particles dispersed in a nonmagnetic carrier liquid [18–20]. It is smart fluid whose properties can be controlled by the magnetic field intensity. In the absence of magnetic field, the properties of the fluid are isotropic, while in the presence of magnetic field the magnetized particles form chain aligned in the direction of the field which results in the appearance of the field-dependent yield stress. Reversible transition from solid to liquid is also possible. Most of MR fluids developed so far have spherical iron particles. Recently, it has been reported

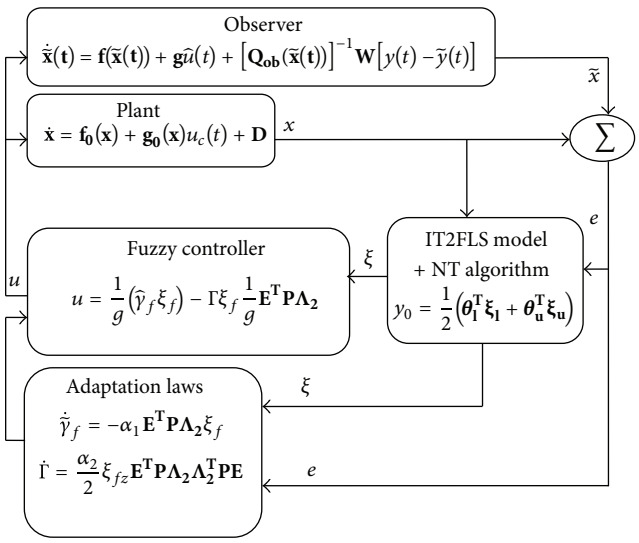

Figure 2: Closed-loop structure of the proposed controller.

that MR fluid containing plate-like iron particles provides better performance than MR fluid featuring spherical iron particle in terms of sedimentation characteristic [21, 22]. Therefore, in this work, a new type of bidisperse MR fluid is used for the application to MR damper. In order to undertake this work, two different sizes of plate-like iron particles are prepared. It consists of iron plate-like particles by weight of two different average diameters suspended in a heavy paraffin oil (64cSt) using mechanical stirrer. Iron microsized particles (Industrial Metal Powder, Pune, India) having average particle size 2 μm (small size) and 19 μm (large size) are used to prepare MR fluid. The structural property of micron-sized magnetic particle is characterized by an X-ray diffractometer, D2-phaser (Bruker XRD, Germany). Bidisperse MR fluid sample is prepared with a variable weight fraction (weigh of small size particles (W_s)/weight of large size particles (W_L)) of 4.00. The particle density is about 7.8 g cm^{-3}. A small amount of stabilizer is then added, stirred, and homogenized for a long time till good dispersion is achieved. Figure 3 shows the X-ray diffraction pattern of plate-like iron particles recorded at room temperature. The XRD result matches with the reported value of *Fe* given in the literature [23]. The magnetization measurement is carried out using a home-built magnetometer. The magnetization saturation of the particles used in this work is about 1250 ± 15 kA m^{-1}. In a field gradient, alignment of the magnetic moment of large size particle is faster compared with the small-sized particle. Under this condition, initial susceptibility and saturation magnetization of larger particles is higher compared with the smaller particle. As a result, the fraction magnetization rises as the weight fraction increases.

Rheological properties in static mode for the MR sample are measured using a Physica MCR 301 (Anton Paar, GmbH, Austria) parallel plate rheometer coupled with a commercial magnetorheological device (MRD 180/1T magnetorheological cell). A diameter of plate is 20 mm and a gap between parallel disks is kept to 1 mm during whole experiment. The magnetic circuit is designed so that the magnetic flux lines are normal to the parallel disk. Magnetic field is perpendicular to the velocity direction. When the magnetic field is applied the shear stress increases quickly with increasing shear rate as shown in Figure 3(a). The shear stress increases with increasing magnetic field strength due to enhancement of magnetic dipole-dipole interactions between the particles. This means that the MR fluid behaves as a Bingham fluid, where a yield stress is needed to initiate flow in the fluid. The Bingham model only applies for the linear portion of the stress-shear rate curve at high shear rate where the suspension flows like a Newtonian liquid [24]. According to this model shear stress is obtained by

$$\tau = \tau_B + \eta_p\dot{\gamma}, \tag{28}$$

where τ is the shear stress, τ_B is the Bingham yield stress caused by the applied magnetic field strength H, and η_P is the field independent plastic viscosity defined as the slope of the shear-stress curve at higher shear rate. The dynamic yield stress value increases with increasing magnetic field strength as shown in Figure 3(b). The data fitted in the second order polynomial equation is expressed as follows:

$$\tau_B = C_0 + C_1H + C_2H^2. \tag{29}$$

In the case of bidisperse suspension of micron-sized magnetic particles due to low applied magnetic field, a pair of short-chain segments forms from the large size particles first. When the external field increases, the substitution of small particles by large particles in a chain would have the effect of weakening the chain structure formed under shearing. The main reason to use bidisperse MR fluid is because it produces a higher yield stress compared with monodisperse suspension. The maximum yield stress generated is 38 kPa at 228 kA m^{-1}. In application point of view, the yield stress is the most important rheological parameter. The sedimentation rate of this MR fluid is 0.3% per day. The characteristics of bidisperse MR fluids are listed in Table 1.

4.2. Model of MR Damper. In this work, a simple dynamic system model installed with MR damper shown in Figure 4 is considered. From Figure 4, the equation of motion can be derived by

$$m\ddot{x}_s + c\dot{x}_s + kx_s = F_s(t), \tag{30}$$

where m is the mass of piston inside damper, c is viscous damping, k is the accumulator stiffness, $F_s(t)$ is external force, and x_s is displacement. The value of c belongs to the damping force of MR damper given by

$$F_{\mathrm{MR}} = \mathrm{sgn}(\dot{x}_1)\, c\,|\dot{x}_1|^{\Theta} = \mathrm{sgn}(x_2)\, c\,|x_2|^{\Theta}, \tag{31}$$

where sgn is signum function, $\Theta \in (0; 1]$. Substituting (31) into (30) and by defining the displacement x_s as a state

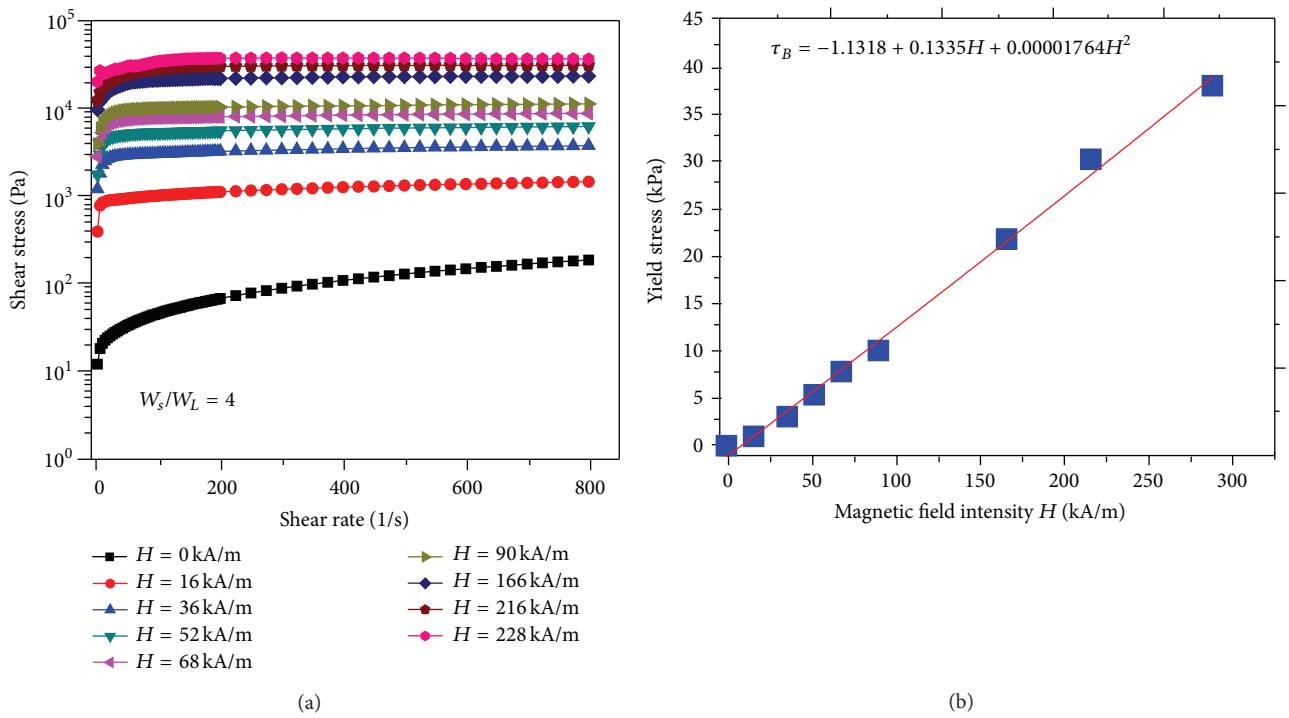

Figure 3: The field-dependent characteristics of the bidisperse MR fluid: (a) shear stress and (b) yield stress.

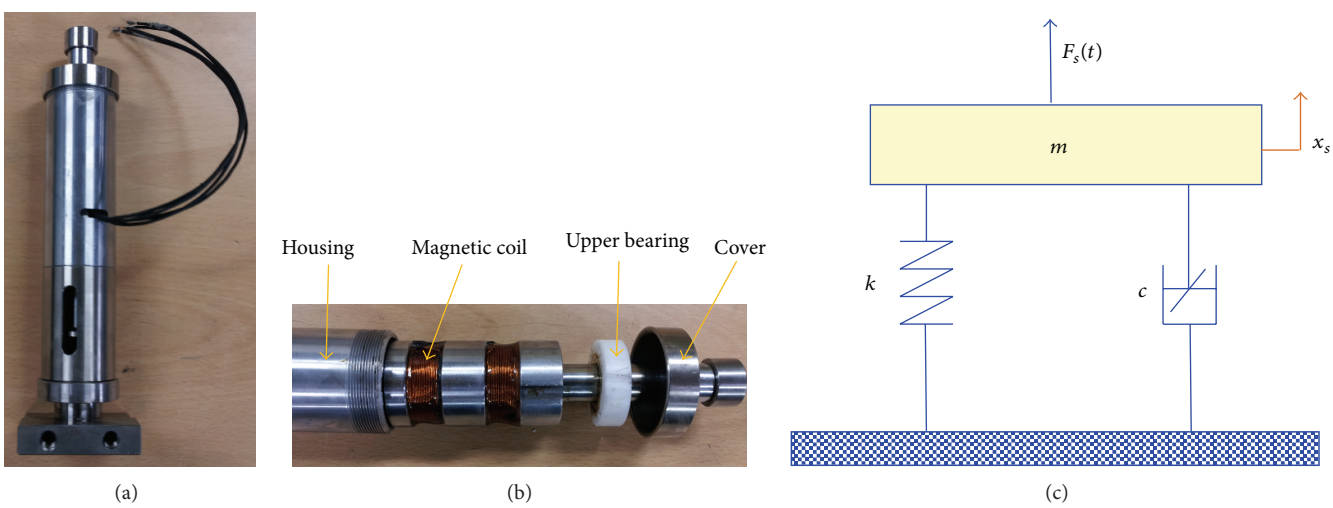

Figure 4: (a) MR damper, (b) inside core of MR damper, and (c) simple mechanical model.

variable x_1 yields the following equation of motion in a state space form:

$$\begin{aligned} \frac{dx_1}{dt} &= x_2, \\ \frac{dx_2}{dt} &= -\frac{k}{m}x_1 - \frac{x_2}{m|x_2|^{\Theta}}F_{\mathrm{MR}}\,\mathrm{sgn}(x_2) + F_s. \end{aligned} \tag{32}$$

From (32), control u_c of the system is expressed by $u_c = F_{\mathrm{MR}}\,\mathrm{sgn}(x_2)$, $f(x) = -(k/m)x_1$, and $g(x) = -\lfloor x_2/(m|x_2|^{\Theta})\rfloor$. To change the system (32) into direct controller, the value θ is chosen by 1. In this application, the semiactive control is applied in damping force control of MR damper. Hence, the damping force due to the yield stress of MR fluid can be expressed as follows [9]:

$$F_{\mathrm{MR}} = \begin{cases} c_{\mathrm{po}}v - F & v \le -v_1,\ \dot{v} > 0 \\ c_{\mathrm{pr}}(v - v_0) & -v_1 \le v \le v_2,\ \dot{v} > 0 \\ c_{\mathrm{po}}v + F & v_2 \le v,\ \dot{v} > 0 \\ c_{\mathrm{po}}v + F & v_1 \le v,\ \dot{v} < 0 \\ c_{\mathrm{pr}}(v + v_0) & -v_2 \le v \le v_1,\ \dot{v} < 0 \\ c_{\mathrm{po}}v - F & v \le -v_2,\ \dot{v} < 0, \end{cases} \tag{33}$$

Table 1: Characteristics of MR fluid.

Properties	Value/limits
Base fluid	Hydrocarbon oil
System	Open or closed
Operating temperature	−23°C to 210°C
Viscosity [Pa·s]	
Shear rate 10 s^{-1}	1.84 Pa·s
Shear rate 80 s^{-1}	0.51 Pa·s
Setting (depend on device design)	The fluid is developed to settle softly and will remix with manual stirring 0.3% per day
Specific heat @ 25°C	
Density	2.04 gm/cm^3
Color	Dark gray
Weight percent of solids	63.82%
Flash point	>150°C

where c_{po} is the postyield viscous damping, c_{pr} is the preyield viscous damping, F is the yield force, v is velocity, v_1 is the decelerating velocity, and v_2 is the accelerating velocity. Values of v_1 and v_2 are found by parameters of c_{po}, c_{pr}, F. The u_c can be seen as the desired damping force of the system. From (32), the control u_c is the semiactive controller for damping force control of MR damper. On the other hand, the observer of the system to estimate the states can be designed by

$$\dot{\tilde{\mathbf{x}}}(t) = \begin{bmatrix} \tilde{x}_2 \\ f(\tilde{x}_1, \tilde{x}_2) \end{bmatrix} + \begin{bmatrix} 0 \\ g \end{bmatrix} u_c(t) + \begin{bmatrix} 1 & 0 \\ 0 & 1 \end{bmatrix} \begin{bmatrix} W_1 \\ W_2 \end{bmatrix} \left[Y - \tilde{Y} \right]. \tag{34}$$

The values of W_1, W_2 are properly chosen by considering both stability and robustness of MR damper control system.

Now, the closed-loop control system for damping force control of MR damper is established as shown in Figure 5. Adaptation laws are used as the outputs of IT2FLS-NT model and the error of system to find adaptive values related f function and Γ in Riccati-like equation. The values of output of adaptation laws are input of the fuzzy controller module. The result of the fuzzy controller is input of damper controller, plant, and observer. It is remarked that damper controller supports the plant (MR damper) in control action. The measured force from the output of plant is used as the input for damper controller and IT2FLS-NT modules. The dynamical responses such as displacement and velocity of plant are used for IT2FLS-NT modules and for calculating error system. On the other hand, the output of the observer is also used for calculating error system and the value of error system is used for the input of IT2FLS-NT model.

Table 2: Centroid and rule of IT2FLS.

(a) Centroid of IT2FLS for controlling MR damper

Rule base	$\mathbf{e}_{21}$	$\mathbf{e}_{22}$
$\mathbf{v}_{11}$	$[-100 \quad -80]$	$[-30 \quad 0]$
$\mathbf{v}_{12}$	$[0 \quad 30]$	$[80 \quad 100]$

(b) Rule table of IT2FLS for controlling MR damper

v/e	NL	NS	PS	PL
NL	1	0.67	0.33	0
NS	0.67	0.33	0	−0.33
PS	0.33	0	−0.33	−0.67
PL	0	−0.33	−0.67	−1

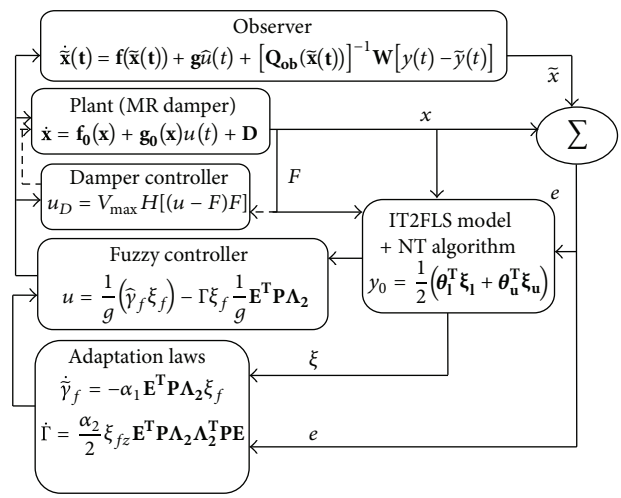

Figure 5: Closed-loop control structure for damping force control of MR damper.

5. Results and Discussions

5.1. Simulation Results. In order to verify high control performance of the proposed direct adaptive fuzzy controller, in this work both computer simulation and experimental realization are undertaken. The fuzzy rules are shown in Tables 2(a) and 2(b). The centroid of four rule bases of IT2FLS is formed by experiment tests based on trial and error method with considering maximal limit of damping force of MR damper. It is here remarked that the relationship between the centroids and rule bases in Table 2(b) has been clearly analyzed in [25, 26] in which the objective of controlled velocities is equal to or less than the exciting velocity, and the error force is also equal to or less than the limited force. The fuzzy models used in this work are shown in Figures 6(a) and 6(b). There are two parameters for these models: velocity of system and error of damping force. The values of fuzzy sets for velocity of $\mathbf{v}_{11}$, $\mathbf{v}_{12}$ and error force of $\mathbf{e}_{21}$, $\mathbf{e}_{22}$ are chosen as follows:

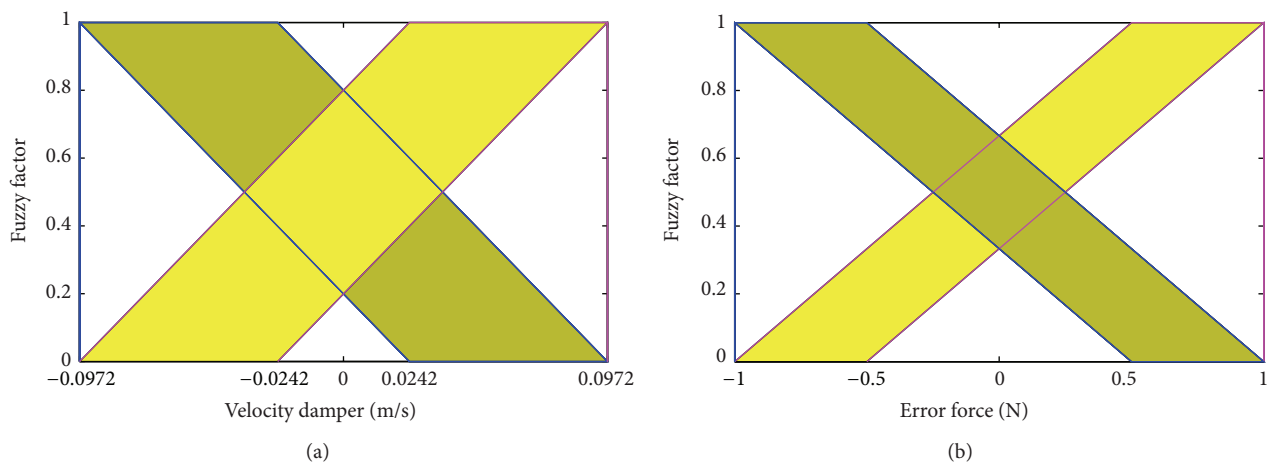

Figure 6: Definition of membership function: (a) velocity and (b) error.

$$\begin{aligned}
\mathbf{v}_{11} &= \left[-0.0972 \quad -0.0972 \quad -0.0242 \quad 0.0972 \quad -0.0972 \quad -0.0972 \quad -0.0972 \quad 0.0242 \quad 1\right] (\mathrm{m/s}), \\
\mathbf{v}_{12} &= \left[-0.0972 \quad 0.0242 \quad 0.0972 \quad 0.0972 \quad -0.0242 \quad 0.0972 \quad 0.0972 \quad 0.0972 \quad 1\right] (\mathrm{m/s}), \\
\mathbf{e}_{21} &= \left[-1 \quad -1 \quad -0.5 \quad 1 \quad -1 \quad -1 \quad -1 \quad 0.5 \quad 1\right] (\mathrm{N}), \\
\mathbf{e}_{21} &= \left[-1 \quad 0.5 \quad 1 \quad 1 \quad -0.5 \quad 1 \quad 1 \quad 1 \quad 1\right] (\mathrm{N}).
\end{aligned} \tag{35}$$

In simulation of the proposed controller, the value Θ is chosen as 1 for direct controller and vector $\mathbf{K} = [1; 6]$. The initial value of Γ is chosen as 10, and the matrix $\mathbf{Q}$ of Riccati-like equation is chosen as $\mathbf{Q} = [-10 \quad 0; 0 \quad -10]$. The constants α_1, α_2 are chosen as 20, 10, respectively. The excited frequency is set by 3 Hz. The matrix $[W_1 \quad W_2]^T$ for observer of the system is used by $[10 \quad 10]^T$. From the relation of damping force and control u_c in (32), the stability and robustness of the system will be evaluated by observing tracking performance of actual damping force to the desired force.

In this simulation, the desired force function for the system is chosen as $F_d = F_D \sin \omega_f t$, where F_D is desired magnitude of force set by $F_D = 70$ N, and ω_f is angular velocity where the frequency of the system f_f is set by 3 Hz. Based on the tracking performance of the damping force, the proposed controller is evaluated in terms of stability and robustness to disturbances. In progress of simulation, the output of control u_c is always evaluated with the desired value of the damping force. This guarantees that the output strictly appears according to the desired value. The external force F_s is chosen as $5 \sin(2\pi f_s t)$ where the frequency f_s is also used as 3 Hz. The initial states of the system are used as $[0 \quad 0.1]$ for both dynamic and observer states. The values of L_f, L_Γ are chosen as 20, 20, respectively. The values of δ_1, δ_2 are used as 0.05, 0.05, respectively. The simulation results on the damping force tracking of the proposed controller are shown in Figure 7. Actual force of the system tracks well the desired damping force as shown in Figures 7(a) and 7(b) which show in 1 cycle. The stability of the system after nearly 60 s is shown in Figure 7(c). In this figure, the time of stability is long because the function $g(x)$ becomes a constant of the system, and the variable control u is applied directly into the system. This progress will take a longer time than indirect adaptive control. The stability is shown in Figure 7(d) in which the velocity of the system becomes small and stable. The applied current of the proposed control in 1 cycle and 100 s is shown in Figures 7(e) and 7(f), respectively. It is seen from Figure 7(a) that the input current is applied in the first time of cycle and holds its value throughout the control process.

In order to highlight good control performance of the proposed controller, a comparative work between the proposed and existing controllers is undertaken. In this work, two existing controllers which are similar to the proposed one are adopted and modified: Tong and Li [1] and Liu and Wang [2]. Adaptation laws in [1, 2] are modified by considering the dynamic model of MR damper which is used in the proposed control system. In simulation for Tong et al. controller, the control vector is used as $\mathbf{K} = [1; 13]$, value of Γ is set by 10, and the initial states of the system are used by $[0.01 \quad 0.1]$ for both dynamic and observer states. The values of L_f, δ_1 are chosen as 20, 0.05, respectively. The control results of Tong et al. controller are shown in Figure 8. It is seen from Figures 8(a) and 8(b) that the actual force is tracking well to the desired force. But the dynamic parameters such as displacement and velocity are unstable as shown in Figures 8(c) and 8(d). This phenomenon is from the performance of adaptation laws of Tong et al. controller

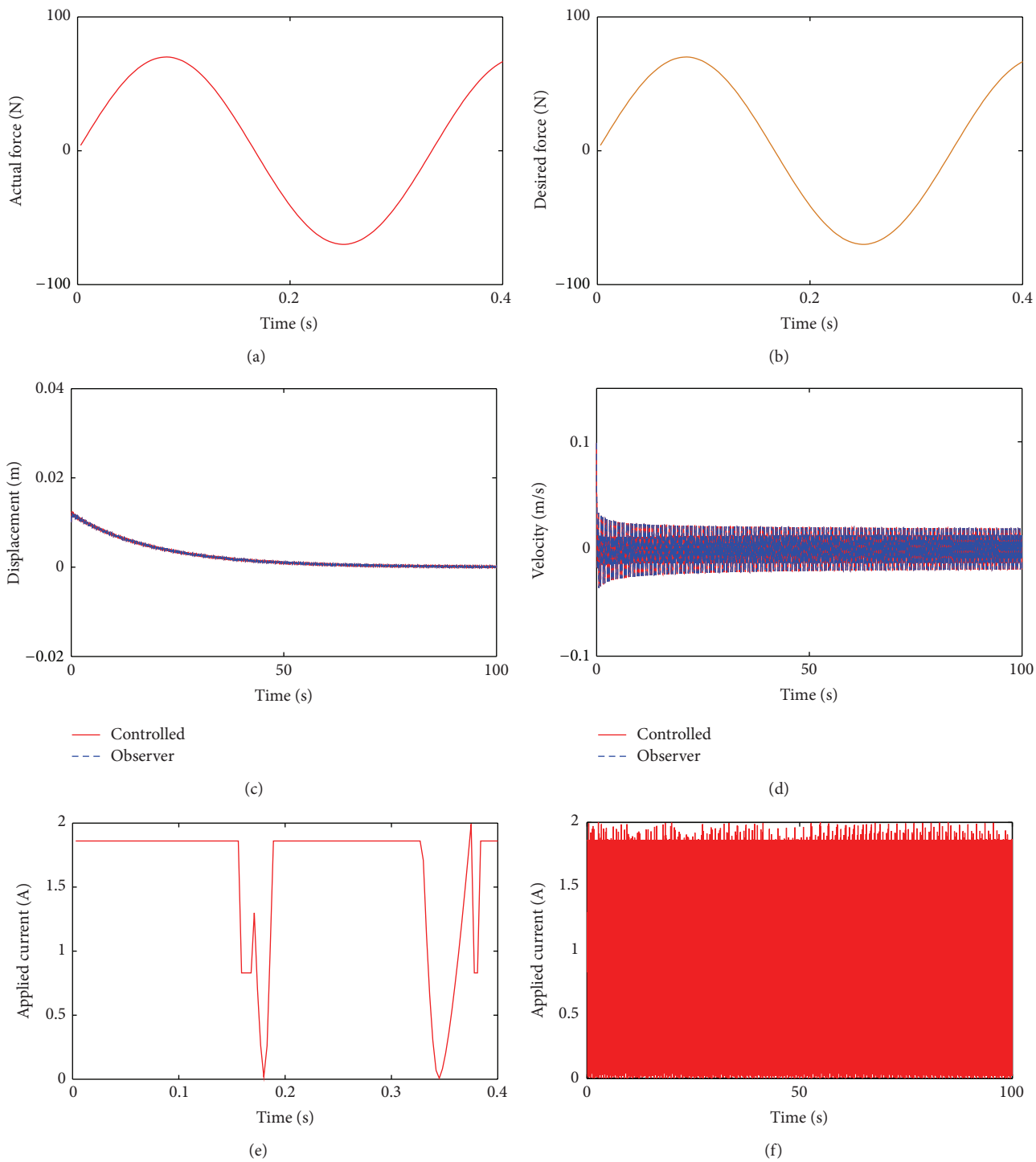

Figure 7: Simulation results at desired force 70 N and excited frequency 3 Hz (proposed controller): (a) actual force, (b) desired force, (c) displacement, (d) velocity, (e) applied current at 1 cycle (for 0.4 s), and (f) applied current for 100 s.

in which all parameters of Riccati-like equation are constant and are not changed through the control process. The applied current of Tong et al. controller is shown in Figures 8(e) and 8(f). It is observed that the results are different from the results shown in Figures 7(e) and 7(f) in which the current input is held and changed a little throughout the control process. The second controller for comparison, Chen et al. controller, is adopted and modified in a same way of Tong et al. controller. It is noted that all setup parameters of Chen et al. controller are similar to Tong et al. controller. The control results of Chen et al. controller are shown in Figure 9. It is observed from results that control results of Chen et al.

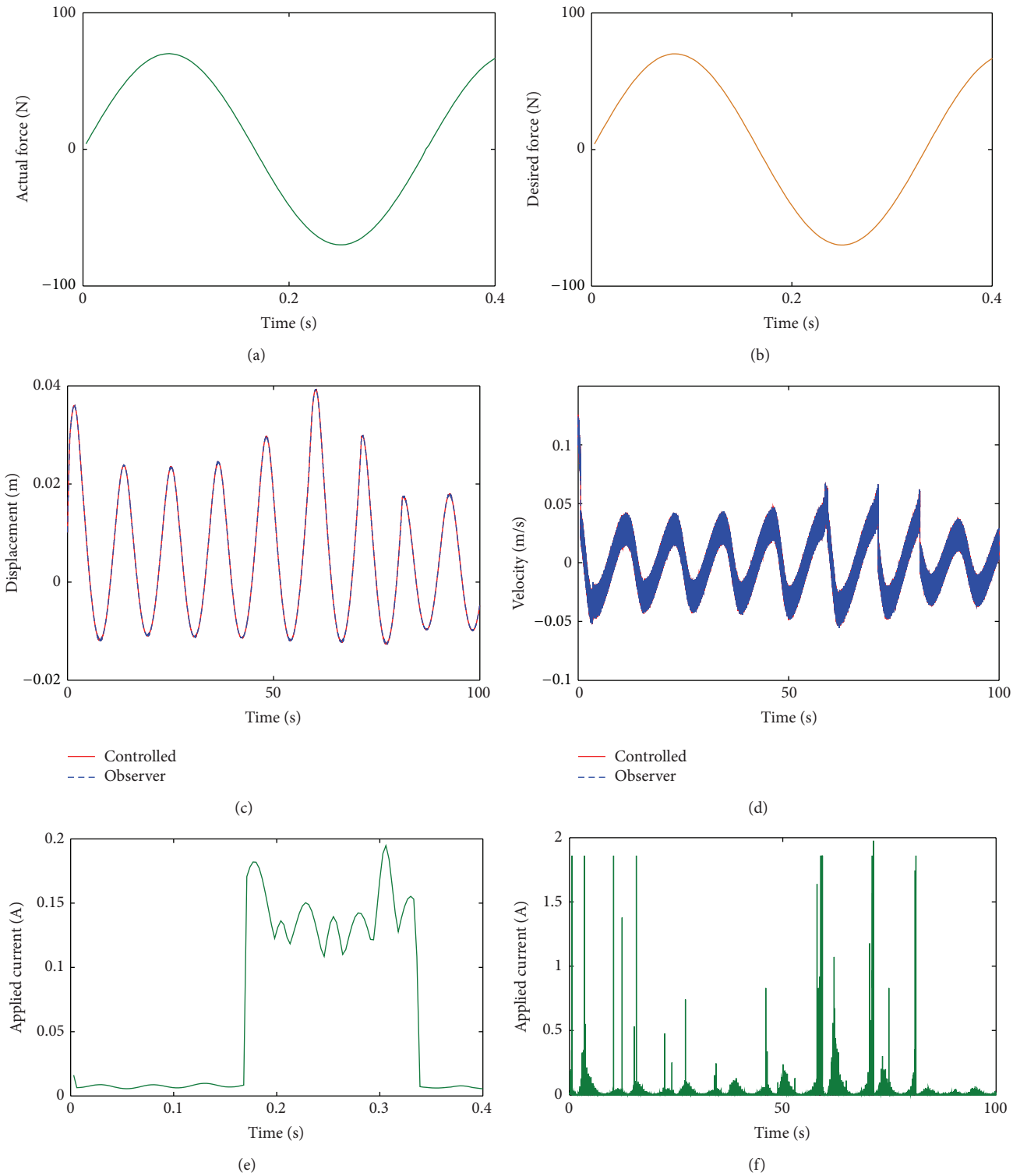

Figure 8: Simulation results at desired force 70 N and excited frequency 3 Hz (Tong et al.'s controller): (a) actual force, (b) desired force, (c) displacement, (d) velocity, (e) applied current at 1 cycle (for 0.4 s), and (f) applied current for 100 s.

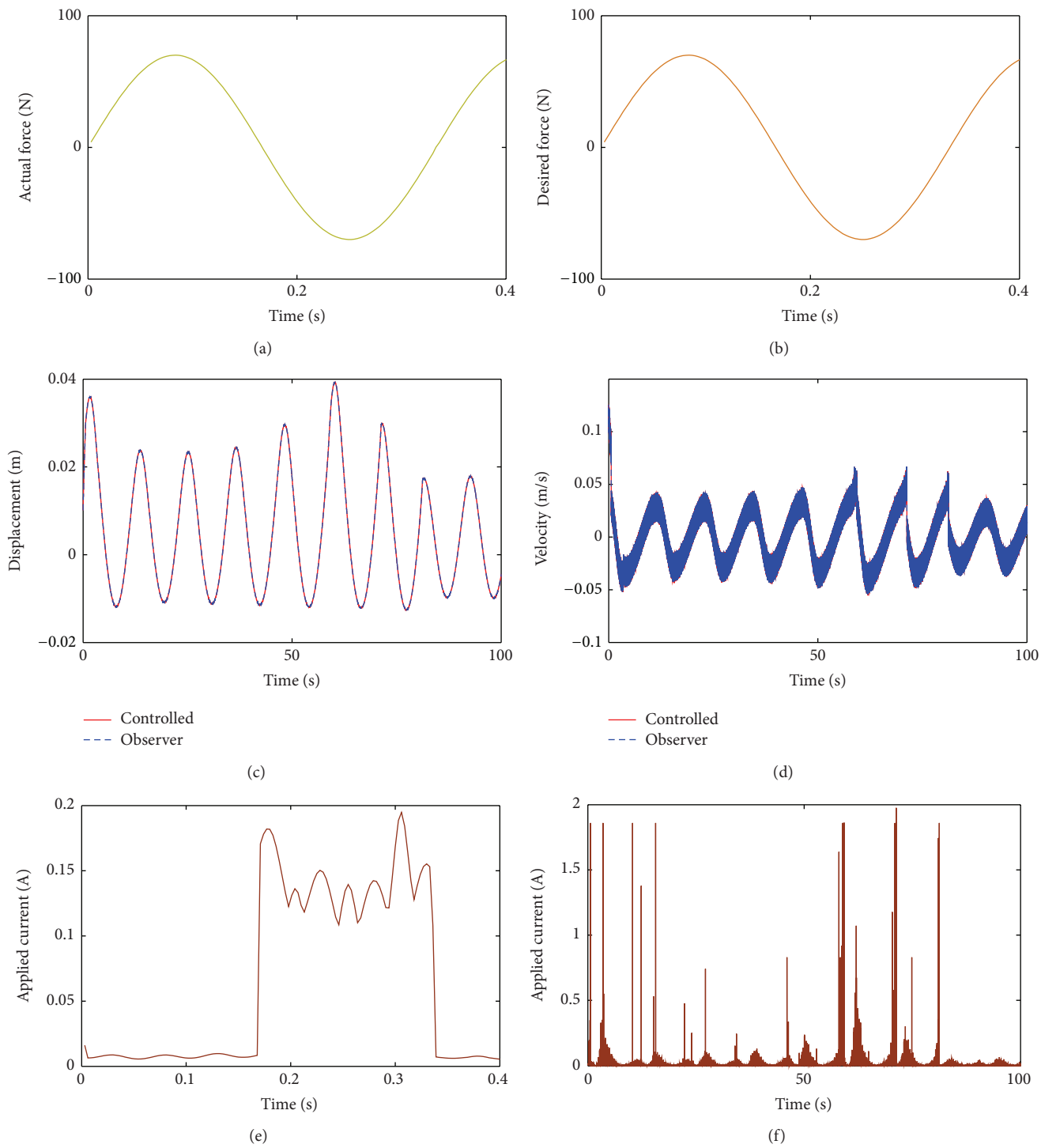

Figure 9: Simulation results at desired force 70 N and excited frequency 3 Hz (Chen et al.'s controller): (a) actual force, (b) desired force, (c) displacement, (d) velocity, (e) applied current at 1 cycle (for 0.4 s), and (f) applied current for 100 s.

controller are almost the same as the Tong et al. controller. The applied currents of Tong et al. controller and Chen et al. controller are similar and the current magnitudes are lower than the proposed controller. This directly indicates that the energy consumption of the proposed controller is larger than the others. However, the proposed controller can guarantee the robustness of the stability during control action, while Tong et al. controller and Chen et al. controller are not sufficient to retain the stability of the system due to the lack of the control robustness. From the above observations, the proposed controller provides much better tracking control performance than Tong et al. controller and Chen et al.

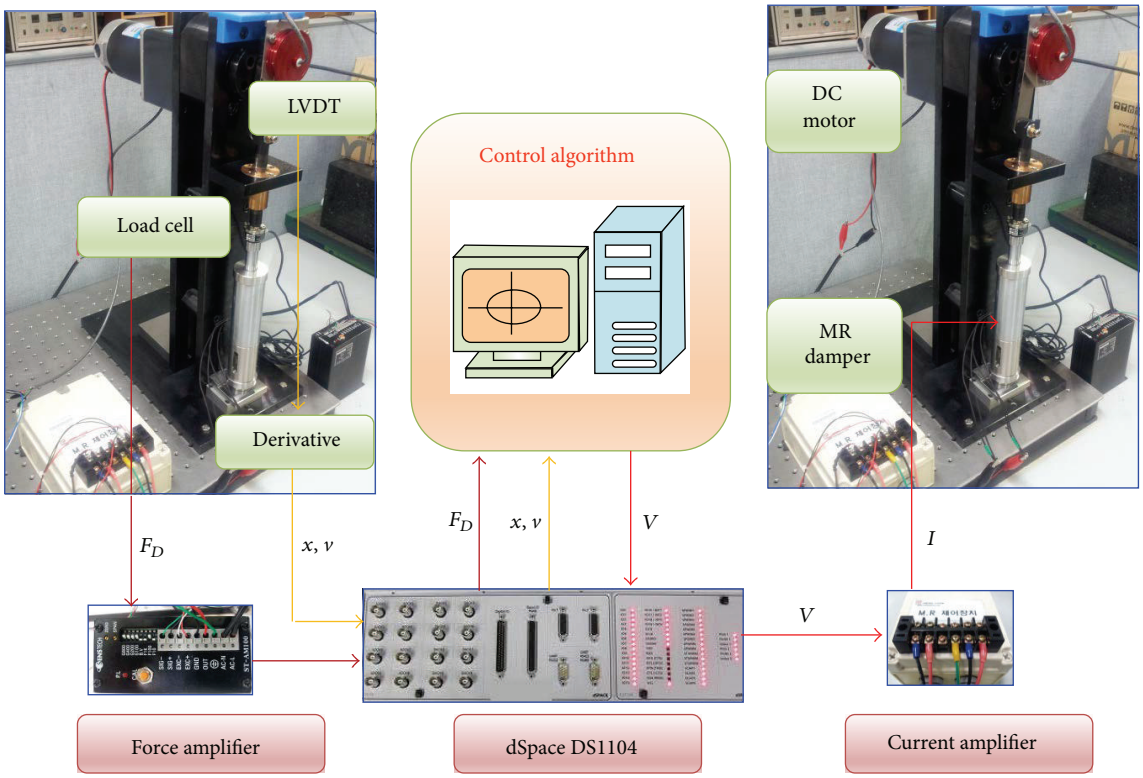

FIGURE 10: Experimental setup for damping force control of MR damper. V: voltage, v: velocity, and I: current.

controller. The proposed controller especially strongly and effectively ensures the robustness against the disturbances resulting in high control performance.

5.2. Experiment Results. In order to more clearly investigate superior control performances of the proposed controller, an experimental apparatus is set up as shown in Figure 10. Force signal is collected by a load cell 20 kgf, and signal force is changed by an amplifier built in dSpace box (DS1104). A wired-type LVDT (Linear Variable Differential Transformer) sensor is used for measuring dynamical response such as displacement and velocity. Exciting vibration is generated by DC motor, and control input from computer system through current amplifier box is applied to MR damper. From (4), the values of c_{po}, c_{pr}, v_0, v_1, v_2 are determined as 941.37 Ns/m, 946.15 Ns/m, 0.073 cm/s, 0.101 cm/s, and 7.436 cm/s, respectively. The control objective in experiment is also to control damping force to follow the desired value.

Control results obtained from experimental realization of the controllers are shown in Figures 11 and 12. The desired force is chosen as 70 N. It is noted that the uncontrolled force (no applied current) and maximal force (maximal applied current) of damper are measured as 21 N and 120 N, respectively. In Figure 11, control results of the proposed controller are shown at four different exciting voltages: 6 V (Voltage), 8 V, 10 V, and 12 V. The exciting frequencies correlative with four voltages are 1.6 Hz, 2.1 Hz, 2.6 Hz, and 3.1 Hz, respectively. It is noted that the exciting voltages indicate the input to be directly applied to the motor. It is seen that controlled force takes nearly 0.04 s to reach the desired force at on-state and 0.08 s at off-state. These times are not changed at four different excited voltages. The positive maximal controlled damping force in Figures 11(a1), 11(b1), 11(c1), and 11(d1) are obtained by 70.998 N, 70.997 N, 70.992 N, and 70.987 N, respectively. The positive minimal controlled damping force in Figures 11(a1), 11(b1), 11(c1), and 11(d1) are 70.098 N, 70.088 N, 70.266 N, and 70.577 N, respectively. The enlarged view of damping forces and control input currents at four excited voltages are shown in Figures 11(a2), 11(a3), 11(b2), 11(b3), 11(c2), 11(c3), 11(d2), and 11(d3). In Figures 11(a2), 11(b2), 11(c2), and 11(d2), it is obviously observed that the stability of the system is not good and hence causes poor tracking performance. It is also seen that the variation of damping force is larger than the proposed controller. From control signals shown in Figures 11(a3), 11(b3), 11(c3), and 11(d3), it is observed that the variation of input current is not large and the maximal control current applied to MR damper is identified by 1.86 A.

For comparison, Tong et al. controller is experimentally realized at same conditions as the controller proposed in this work. The control results are shown in Figure 12. The excited voltages are the same as the proposed controller as 6 V, 8 V, 10 V, and 12 V. The positive maximal controlled damping force in Figures 12(a1), 12(b1), 12(c1), and 12(d1) are obtained by 74.941 N, 73.916 N, 73.964 N, and 73.914 N, respectively. The positive minimal controlled damping force in Figures 12(a1), 12(b1), 12(c1), and 12(d1) are identified by 62.051 N, 63.490 N, 61.758 N, and 62.458 N, respectively. The enlarged

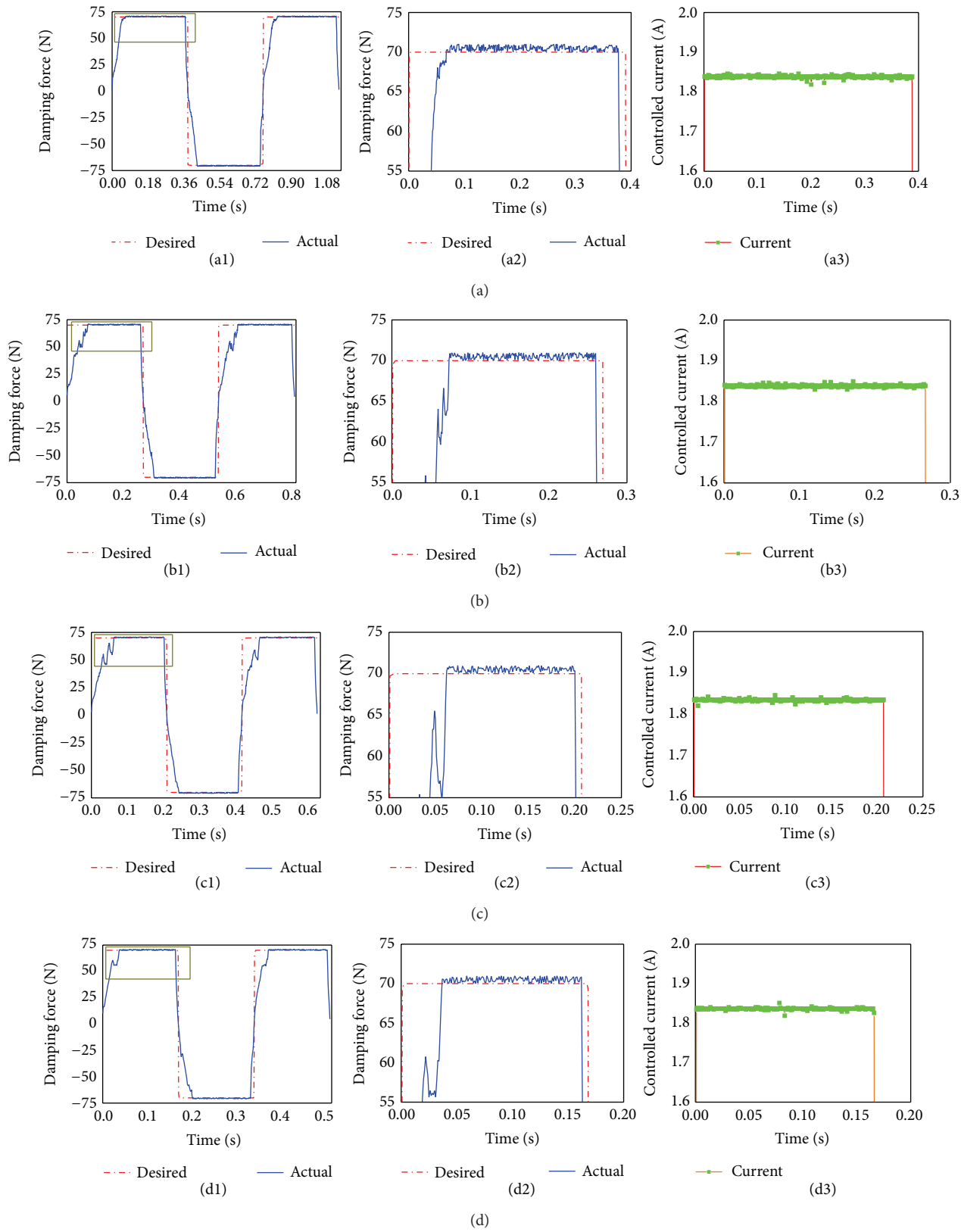

Figure 11: Experiment results of the proposed controller: (a1) damping force versus time at 6 V (Voltage), (a2) amplification of a's view, (a3) current at 6 V, (b1) damping force versus time at 8 V, (b2) amplification of b's view, (b3) current at 8 V, (c1) damping force versus time at 10 V, (c2) amplification of c's view, (c3) current at 10 V, (d1) damping force versus time at 12 V, (d2) amplification of d's view, and (d3) current at 10 V.

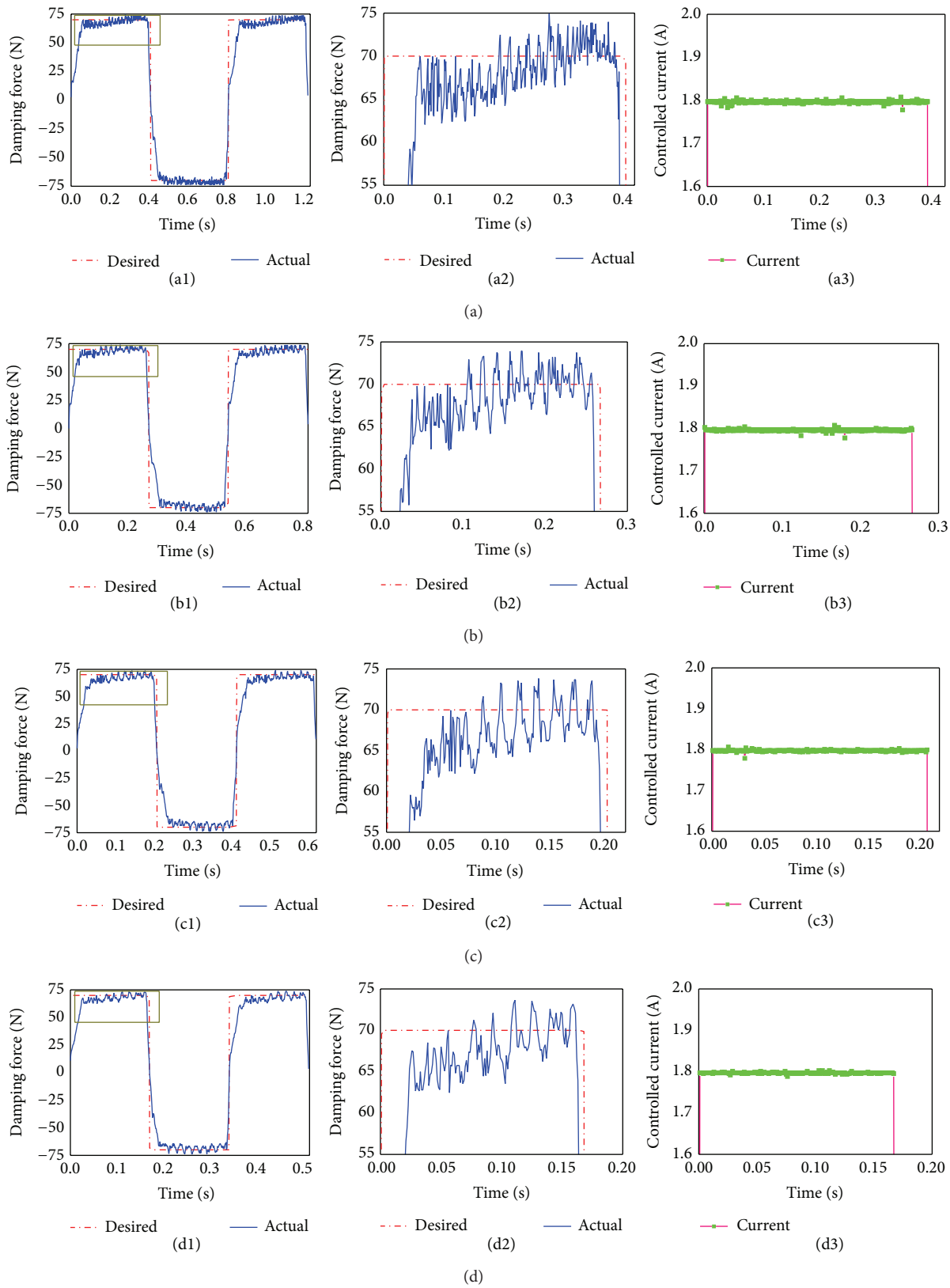

Figure 12: Experiment results of Tong et al. controller: (a1) damping force versus time at 6 V, (a2) amplification of a's view, (a3) current at 6 V, (b1) damping force versus time at 8 V, (b2) amplification of b's view, (b3) current at 8 V, (c1) damping force versus time at 10 V, (c2) amplification of c's view, (c3) current at 10 V, (d1) damping force versus time at 12 V, (d2) amplification of d's view, and (d3) current at 10 V.

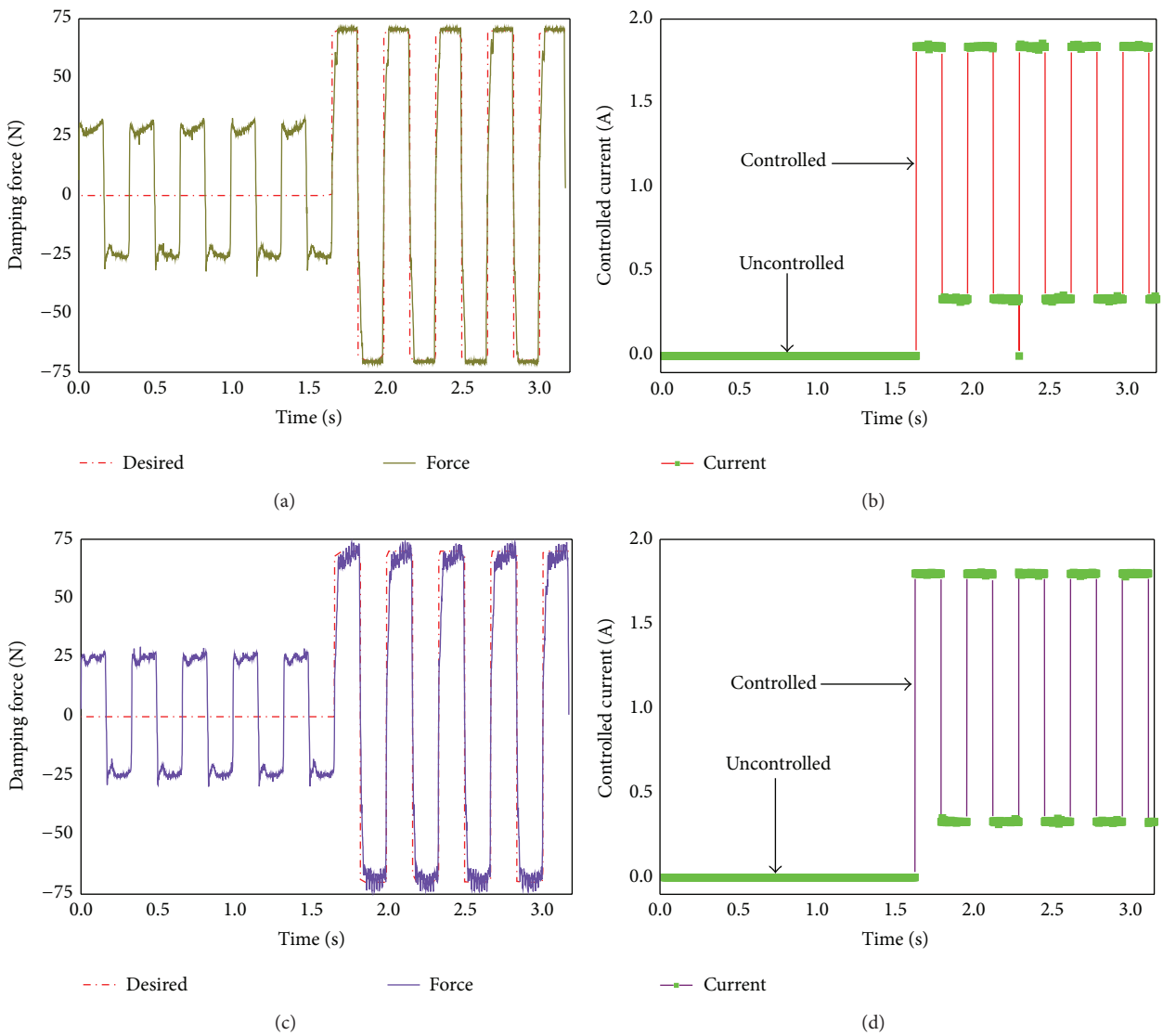

Figure 13: Damping force (DF) and controlled current (CR) of two controllers: (a) DF of proposed controller at 12 V, (b) CR of proposed controller at 12 V, (c) DF of Tong et al. controller at 12 V, and (d) CR of Tong et al. controller at 12 V.

view of damping forces and control input currents for four excited voltages are shown in Figures 12(a2), 12(a3), 12(b2), 12(b3), 12(c2), 12(c3), 12(d2), and 12(d3). In Figures 12(a2), 12(b2), 12(c2), and 12(d2), it is obviously observed that the stability of the system is not good, and hence this result in poor tracking performance. It is also seen that the variation of damping force is larger than the proposed controller. This indicates that Tong et al. controller cannot sufficiently control the disturbances and hence the robustness of the system is not fully guaranteed. From the input histories shown in Figures 12(a3), 12(b3), 12(c3), and 12(d3), it is seen that the variation of the control current is not large and the maximal control current is 1.83 A. Figure 13 presents tracking performance of damping force and corresponding applied control input. The positive force and negative force controlled with two different controllers are nearly 27 N and −27 N, respectively. It is clearly seen that the proposed controller is much better than Tong et al. controller in term of tracking performance of damping force. This is because the proposed controller has adaptation law to overcome external disturbances, while Tong et al. controller does not have it.

6. Conclusion

In this work, a new direct adaptive fuzzy controller was developed and its superior control performance was verified through both simulation and experiment associated with MR damper system. The proposed controller was developed based on model of interval type 2 fuzzy and H^{∞} tracking technique. For performance verification, MR damper containing plate-like iron particles was adopted and its damping force tracking was evaluated. In addition, two existing controllers of Tong et al. and Chen et al. were adopted and modified for comparative work with the proposed controller.

Control results achieved from simulation and experiment demonstrate that the proposed controller is much better than the others in terms of stability and robustness. This directly indicates the enhancement of damping force tracking performance of the filed-dependent damping force of MR damper of the proposed controller and hence excellent vibration control performance has been achieved. It has been also observed that Tong et al. controller and Chen et al. controller are not converged well and hence cannot sufficiently guarantee the robustness against the disturbance. It is finally remarked that the proposed direct adaptive fuzzy controller can be effectively utilized to numerous MR application control systems subjected to uncertainties or/and disturbances without significant modification.

Conflict of Interests

The authors declare that there is no conflict of interests.

Acknowledgment

This work was supported by a National Research Foundation of Korea (NRF) grant funded by the Korean Government (MEST) (no. 2010-0015090). This financial support is gratefully acknowledged.

References

[1] S. Tong and H.-X. Li, "Direct adaptive fuzzy output tracking control of nonlinear systems," *Fuzzy Sets and Systems*, vol. 128, no. 1, pp. 107–115, 2002.

[2] Y.-J. Liu and W. Wang, "Adaptive fuzzy control for a class of uncertain nonaffine nonlinear systems," *Information Sciences*, vol. 177, no. 18, pp. 3901–3917, 2007.

[3] S. Sui, S. Tong, and Y. Li, "Observer-based adaptive fuzzy decentralized control for stochastic large-scale nonlinear systems with unknown dead-zones," *Information Sciences*, vol. 259, pp. 71–86, 2014.

[4] Y. Li, S. Tong, and T. Li, "Adaptive fuzzy output-feedback control for output constrained nonlinear systems in the presence of input saturation," *Fuzzy Sets and Systems*, vol. 248, pp. 138–155, 2014.

[5] F. Yang, R. Yuan, J. Yi, G. Fan, and X. Tan, "Direct adaptive type-2 fuzzy logic control of a generic hypersonic flight vehicle," in *Proceedings of the 4th International Conference on Intelligent Control and Information Processing (ICICIP '13)*, pp. 581–586, Beijing, China, June 2013.

[6] C.-W. Chen, K. Yeh, K. F. Liu, and M.-L. Lin, "Applications of fuzzy control to nonlinear time-delay systems using the linear matrix inequality fuzzy Lyapunov method," *Journal of Vibration and Control*, vol. 18, no. 10, pp. 1561–1574, 2012.

[7] D. X. Phu, N. V. Quoc, J.-H. Park, and S.-B. Choi, "Design of a novel adaptive fuzzy sliding mode controller and application for vibration control of magnetorheological mount," *Proceedings of the Institution of Mechanical Engineers Part C: Journal of Mechanical Engineering Science*, vol. 228, no. 13, pp. 2285–2302, 2014.

[8] S. D. Nguyen and S.-B. Choi, "A novel minimum-maximum data-clustering algorithm for vibration control of a semi-active vehicle suspension system," *Proceedings of the Institution of Mechanical Engineers, Part D: Journal of Automobile Engineering*, vol. 227, no. 9, pp. 1242–1254, 2013.

[9] N. M. Wereley, L. Pang, and G. M. Kamath, "Idealized hysteresis modeling of electrorheological and magnetorheological dampers," *Journal of Intelligent Material Systems and Structures*, vol. 9, no. 8, pp. 642–649, 1998.

[10] S. J. Dyke, B. F. Spencer Jr., M. K. Sain, and J. D. Carlson, "Modeling and control of magnetorheological dampers for seismic response reduction," *Smart Materials and Structures*, vol. 5, no. 5, pp. 565–575, 1996.

[11] F. Weber and M. Maślanka, "Precise stiffness and damping emulation with MR dampers and its application to semi-active tuned mass dampers of Wolgograd Bridge," *Smart Materials and Structures*, vol. 23, no. 1, Article ID 015019, 2014.

[12] R. Russo and M. Terzo, "Modelling, parameter identification, and control of a shear mode magnetorheological device," *Proceedings of the Institution of Mechanical Engineers. Part I: Journal of Systems and Control Engineering*, vol. 225, no. 5, pp. 549–562, 2011.

[13] D. Wu, "Approaches for reducing the computational cost of interval type-2 fuzzy logic systems: overview and comparisons," *IEEE Transactions on Fuzzy Systems*, vol. 21, no. 1, pp. 80–99, 2013.

[14] J. M. Mendel, "On KM algorithms for solving type-2 fuzzy set problems," *IEEE Transactions on Fuzzy Systems*, vol. 21, no. 3, pp. 426–446, 2013.

[15] J. M. Mendel and X. Liu, "Simplified interval type-2 fuzzy logic systems," *IEEE Transactions on Fuzzy Systems*, vol. 21, no. 6, pp. 1056–1069, 2013.

[16] Y. V. Orlov and L. T. Aguilar, *Advanced* H_∞ *Control Towards Nonsmooth Theory and Applications*, Birkhäauser, New York, NY, USA, 2014.

[17] G. Ciccarella, M. Dalla Mora, and A. Germani, "A Luenberger-like observer for nonlinear systems," *International Journal of Control*, vol. 57, no. 3, pp. 537–556, 1993.

[18] G. Bossis, S. Lacis, A. Meunier, and O. Volkova, "Magnetorheological fluids," *Journal of Magnetism and Magnetic Materials*, vol. 252, no. 1–3, pp. 224–228, 2002.

[19] J.-I. Takimoto, K. Minagawa, and K. Koyama, "Numerical study of the response time of ER suspensions," *International Journal of Modern Physics B*, vol. 10, no. 23-24, pp. 3037–3044, 1996.

[20] O. Volkova, G. Bossis, M. Guyot, V. Bashtovoi, and A. Reks, "Magnetorheology of magnetic holes compared to magnetic particles," *Journal of Rheology*, vol. 44, no. 1, pp. 91–104, 2000.

[21] K. Shah, J.-S. Oh, S.-B. Choi, and R. V. Upadhyay, "Plate-like iron particles based bidisperse magnetorheological fluid," *Journal of Applied Physics*, vol. 114, no. 21, Article ID 213904, 2013.

[22] K. Shah, D. X. Phu, and S. B. Choi, "Rheological properties of bi-dispersed magnetorheological fluids based on plate-like iron particles with application to a small-sized damper," *Journal of Applied Physics*, vol. 115, no. 20, Article ID 203907, 2014.

[23] J. de Vicente, V. Fernando, J. P. Segovia-Gutiérrez, M. D. P. Morales, and R. Hidalgo-Álvarez, "Effect of particle shape in magnetorheology," *Journal of Rheology*, vol. 54, pp. 1337–1362, 2010.

[24] B.-J. de Gans, H. Hoekstra, and J. Mellema, "Non-linear magnetorheological behaviour of an inverse ferrofluid," *Faraday Discussions*, vol. 112, pp. 209–224, 1999.

[25] K. M. Passino, *Biomimicry for Optimization, Control, and Automation*, Springer, London, UK, 2005.

[26] D. Wu, *Design and analysis of type 2 fuzzy logic systems [M.S. thesis]*, National University of Singapore, 2005.